Brine fluxes from growing sea ice

A. J. Wells,[1,2] J. S. Wettlaufer,[1,2,3] and S. A. Orszag[2,4]

Received 24 November 2010; revised 6 January 2011; accepted 14 January 2011; published 26 February 2011.

[1] It is well known that brine drainage from growing sea ice has a controlling influence on its mechanical, electromagnetic, biological and transport properties, and hence upon the buoyancy forcing and ecology in the polar oceans. When the ice has exceeded a critical thickness the drainage process is dominated by brine channels: liquid conduits extending through the ice. We describe a theoretical model for the drainage process using mushy layer theory which demonstrates that the brine channel spacing is governed by a selection mechanism that maximizes the rate of removal of stored potential energy, and hence the brine flux from the system. The fluid transport through the sea ice and hence the scaling laws for brine fluxes and brine channel spacings are predicted. Importantly, the resulting brine flux scaling is consistent with experimental data for growth from a fixed temperature surface, allowing all parameters in the scaling law to be determined. This provides an experimentally tested first principles derivation of a parameterization for brine fluxes from growing sea ice. **Citation:** Wells, A. J., J. S. Wettlaufer, and S. A. Orszag (2011), Brine fluxes from growing sea ice, *Geophys. Res. Lett.*, *38*, L04501, doi:10.1029/2010GL046288.

1. Introduction

[2] The spatio-temporal distribution of the liquid phase within sea ice, a porous array of ice crystals interspersed with liquid brine, underlies all of its physical and biological properties (see *Weeks* [2010] and *Thomas and Dieckmann* [2010] for reviews). It is evident that a first principles understanding of the processes associated with the fate of brine is required to provide physically based approximations for geophysical-scale modeling. As the ice cover evolves, salt is lost to the ocean primarily by gravity drainage in winter, and flushing by surface meltwater in summer [*Untersteiner*, 1968]. The desalination process modifies the porosity of sea ice, the transport of passive scalars, such as heat, gases and nutrients through it and hence has a controlling influence on the biota within, and in proximity to, the ice cover [*Thomas and Dieckmann*, 2010]. Whereas theoretical estimates of the salinity structure of perennial sea ice are in good agreement with observations [*Untersteiner*, 1968], this is not the case for first year ice [*Notz et al.*, 2005]. The brine flux emanating from sea ice controls the surface buoyancy forcing of the polar oceans, with first year sea ice growth extending over approximately 8×10^6 km^2 in the Arctic, and 1.5×10^7 km^2 in the Antarctic [*Comiso*, 2003]. Hence, a fundamental understanding of this basic process is a key component of polar climate dynamics and ice ecology. We address the principal aspects of the brine flux problem in first year ice here.

[3] Field measurements reviewed by *Weeks* [2010] show that the bulk salinity of sea ice evolves over time and space, from the upper ocean salinity of order 35 ppt at the base of a newly formed layer to a bulk value of approximately 3 ppt in multiyear ice. First year sea ice is typically characterized by a "C-shaped" profile. In the early stages of growth, a region of high permeability, often called the "skeletal layer", is observed in the lowermost few centimeters of the ice from which convective gravity drainage removes dense brine [e.g., *Eide and Martin*, 1975]. However, once the sea ice thickness exceeds ~5–10 cm the convective downflow is dominated by brine channels – near-vertical conduits devoid of ice through which plumes of dense brine drain into the underlying ocean. Post mortems reveal mean brine channel spacings are comparable to the depth of the convecting layer at the base of the ice [*Lake and Lewis*, 1970; *Eide and Martin*, 1975; *Wakatsuchi and Saito*, 1985; *Notz and Worster*, 2009]. Laboratory experiments reveal the same features. As is to be expected, brine fluxes vary depending on the thermal boundary conditions and growth rate [*Foster*, 1969; *Wakatsuchi and Ono*, 1983; *Cox and Weeks*, 1988; *Wettlaufer et al.*, 1997]. Early stages of thermohaline convection were visualized long ago [*Foster*, 1969] and more recently experiments have closed the mass budget while examining the stages of the flow regimes associated with the spatio-temporal variation of the ice porosity to test the basic conservation laws of this dynamic two-phase system [*Wettlaufer et al.*, 1997].

[4] Theoretical studies of gravity drainage rely either on an empirical parameterization using an effective segregation coefficient [*Cox and Weeks*, 1988], or prescribe a diffusive mixing process using an enhanced artificial diffusivity that is some function of the local Rayleigh number [*Vancoppenolle et al.*, 2009]. Some two dimensional models of brine transport offer evidence of localized brine drainage features, but lack the sub-millimeter scale resolution required to accurately describe liquid flow in the brine channels. Predictive capability requires a more general theoretical framework which recognizes that sea ice is a chemically reacting porous medium, most generally referred to as a mushy layer [*Feltham et al.*, 2006]. Experimental work on convection in mushy layers undergoing transient growth reveals an increase in the mean spacing between brine channels as the mushy region thickens over time [*Tait and Jaupart*, 1992; *Solomon and Hartley*, 1998]. Theoretical

[1]Department of Geology and Geophysics, Yale University, New Haven, Connecticut, USA.
[2]Program in Applied Mathematics, Yale University, New Haven, Connecticut, USA.
[3]Department of Physics, Yale University, New Haven, Connecticut, USA.
[4]Department of Mathematics, Yale University, New Haven, Connecticut, USA.

0094-8276/11/2010GL046288

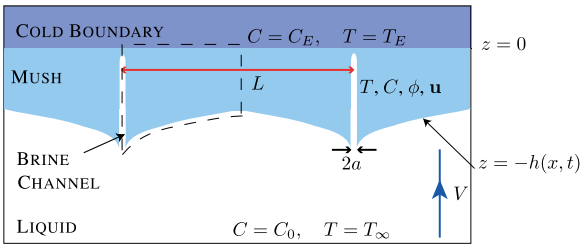

Figure 1. Water of far-field salinity C_0 and temperature T_∞ is translated upward at a rate V towards an upper cooled boundary at the eutectic temperature T_E and salinity C_E. The resulting mushy region has an array of brine channels of imposed spacing L, and we exploit symmetry to solve for the evolution of the region of mushy layer indicated by the dashed outline.

and experimental work on mushy layers has identified conditions for the onset of convection in a variety of settings predicting the formation and evolution of brine channels [e.g., *Worster*, 1992; *Wettlaufer et al.*, 1997; *Schulze and Worster*, 1998; *Chung and Worster*, 2002; *Katz and Worster*, 2008; *Neufeld and Wettlaufer*, 2008]. Recently, we have demonstrated that brine channel spacing is governed by a variational principal in which the rate of removal of stored potential energy is maximized [*Wells et al.*, 2010]. Here, we apply this analysis to develop a physically based description of brine fluxes from sea ice that collapses a wide range of experimental data.

2. A Model of Ice Growth

[5] We treat the solidification process by considering salt water of salinity C_0 translated vertically upward at a mean solidification rate V between two heat baths at temperatures T_∞ and T_E, as illustrated in Figure 1, where the eutectic point has temperature T_E and salinity C_E. The liquid partially solidifies to form a mushy region with a porous array of ice crystals bathed in dense salt enriched brine that undergoes buoyancy driven convection. One can think of this system as analogous to a convecting region of fixed depth within the sea ice layer and evolving over time to follow the mush liquid interface as seen experimentally [*Notz and Worster*, 2009]. We model the observations of well developed convection from brine channels in a periodic array with spacing L. Time dependent mushy layer theory [*Schulze and Worster*, 2005] is used to solve for the Darcy velocity $\mathbf{u}$, temperature T, volume fraction of solid ϕ and liquid salinity C within the mushy region of thickness $h(x, t)$, and we also solve for the brine channel width $a(z, t)$. The theory conserves heat and salt, invoking a condition of local thermodynamic equilibrium (with the freezing temperature depending linearly on salinity) to determine the local solid fraction, and evolving the mush-liquid free boundaries to satisfy the condition of marginal equilibrium so that the solid grows sufficiently to just eliminate any constitutional supercooling in the liquid. Fluid flow in the porous layer is described by Darcy's law driven by pressure gradients and buoyancy forces, and asymptotic approximations are applied to describe the flow within brine channels and the underlying liquid, as well as to provide boundary conditions for the mushy region. The conservation equations and boundary conditions were integrated using second-order finite differences, with heat and salinity equations treated using semi-implicit Crank-Nicolson time-stepping. The resulting equations for the fluid stream function and dimensionless temperature were solved using multigrid iteration [*Briggs et al.*, 2000; *Adams*, 1989] and $h(x, t)$ and $a(z, t)$ were updated using relaxation (see *Wells et al.* [2010], for more details).

[6] The system is characterized by the dimensionless parameters

$$\mathrm{R_m} = \frac{\rho_0 g \beta \Delta C \Pi_0 l_T}{\mu \kappa}, \quad \mathcal{C} = \frac{C_0 - C_S}{\Delta C}, \quad \mathrm{Da} = \frac{\Pi_0 V^2}{\kappa^2},$$
$$\theta_\infty = \frac{T_\infty - T_L(C_0)}{\Gamma \Delta C}, \quad \mathcal{S} = \frac{L}{c_p \Gamma \Delta C}, \quad \lambda = \frac{VL}{2\kappa}, \tag{1}$$

where $\Delta C = C_E - C_0$, $l_T = \kappa/V$, κ is the thermal diffusivity, $T_L(C_0)$ is the liquidus temperature of the underlying liquid,

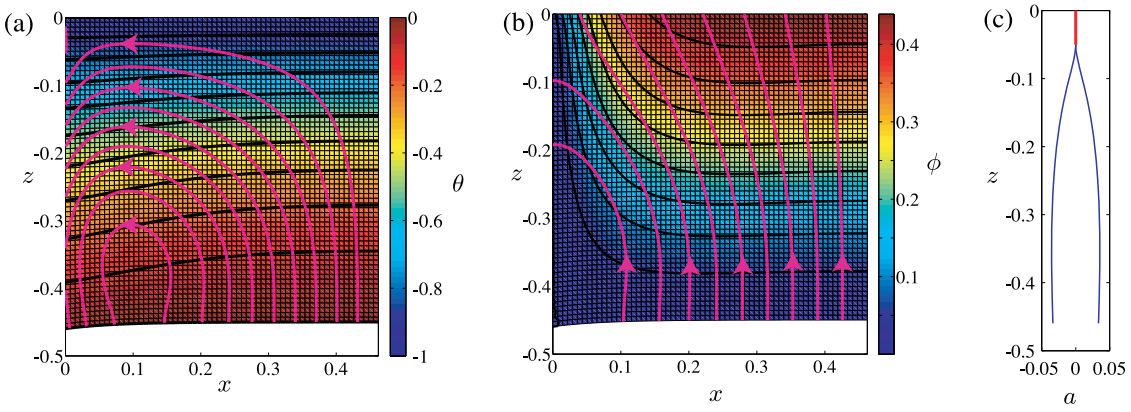

Figure 2. Profiles of (a) dimensionless temperature $\theta = [T - T_L(C_0)]/\Gamma\Delta C$ shown by color scale with isotherms as black curves, and streamlines of Darcy velocity (relative to the stationary ice crystal matrix) shown as magenta curves; (b) solid fraction ϕ shown by color scale with constant ϕ contours in black, and streamlines of material flux relative to the freezing ice-water interface in magenta; and (c) brine channel width $2a(z)$. The brine channel is located at $x = 0$ and parameterized as a singular-interface boundary condition in the numerical model. Plots are for $\mathcal{C} = 2$, $\mathrm{R_m} = 50$, $\theta_\infty = 0.4$, $\mathcal{S} = 5$ and $\mathrm{Da} = 5 \times 10^{-3}$, but a similar structure is observed for other values of $2 \le \mathcal{C} \le 15$ and $30 \le \mathrm{R_m} \le 60$. Numerical difficulties make continuation to smaller values of $\mathcal{C}$ challenging.

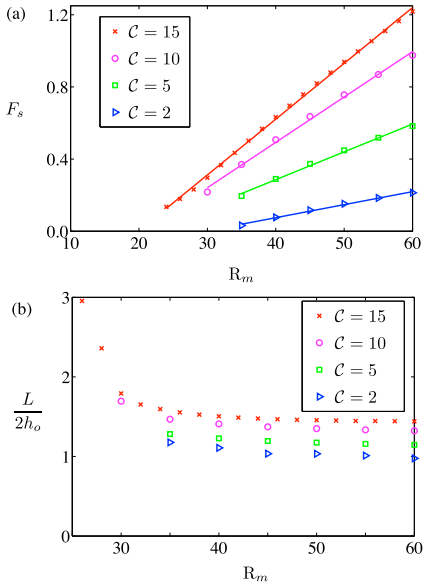

Figure 3. Variation with Rayleigh number R_m of (a) the dimensionless brine flux F_s and (b) ratio of brine channel spacing L to minimum mushy layer depth $h_o = h(\lambda)$, for a range of salinity ratios $\mathcal{C}$. For each salinity ratio, the flux can be approximated by a piecewise linear trend $F_s = 0$ for $R_m < R_c$ and $F_s = \gamma (R_m - R_c)$ for $R_m > R_c$ (best fit lines shown), and the aspect ratio $L/2h_o$ approaches a constant value for $R_m \gg R_c$.

C_S is the solid concentration, Π_0 is a characteristic permeability, ρ_0 is the fluid density, β is the haline expansion coefficient, g is the gravitational acceleration c_p is the specific heat, μ is the dynamic viscosity and Γ is the freezing point depression (or liquidus slope in the materials science parlance). The mushy-layer Rayleigh number R_m characterizes the ratio of buoyancy forces to dissipation, the Darcy number Da captures the permeability of the porous layer, and the concentration or salinity ratio $\mathcal{C}$, Stefan number $\mathcal{S}$ and scaled far-field temperature θ_∞ characterize the thermal and solutal conditions imposed on the system.

[7] The brine channel spacing L is dynamically selected to maximize the release rate of potential energy from the system, thereby yielding an optimal solute flux [*Wells et al.*, 2010]. Indeed, this variational principal predicts convection in cells with an aspect ratio of order one as shown in Figure 2 for $\mathcal{C} = 2$, with profiles of this structure obtained throughout the range $2 \le \mathcal{C} \le 15$. While the salinity ratios used are larger than the value $\mathcal{C} \approx 0.15$ found in sea ice, the streamlines of Darcy velocity (Figure 2a, and calculations not shown) demonstrate that this form of convection persists for a wide range of $\mathcal{C}$. This clearly supports the notion that gravity drainage in sea ice is mediated by similar convection cells in the most permeable region within the system where convection is active. This convection drives fluid exchange with the underlying ocean, with streamlines of material flux relative to the ice-water interface (Figure 2b) showing inflow at the base of the ice and outflow via the brine channel at $x = 0$. Figure 2b also shows significant spatial variation of the solid fraction ϕ, which creates local variations in the structural properties of sea ice.

[8] In Figure 3 we show how the optimal dimensionless brine flux and brine channel spacing vary with Rayleigh number for a wide range of $\mathcal{C}$. Brine channels close up and the brine flux vanishes for Rayleigh numbers less than a critical value $R_m < R_c$, whereas for $R_m > R_c$, convection controlled by brine channels yields a flux that increases approximately linearly with Rayleigh number for $R_c \ll R_m \le 60$. This is consistent with the dimensional brine flux scaling

$$F = \gamma \frac{\rho_0 g \beta (C_E - C_0)^2 \Pi_0}{\mu} \left(\frac{R_m - R_c}{R_m} \right), \qquad \text{for} \quad R_m > R_c$$
$$F = 0, \qquad \text{for} \quad R_m < R_c \tag{2}$$

that was previously determined for $\mathcal{C} = 15$ [*Wells et al.*, 2010], where γ is a constant to be determined in the analysis that follows. Figure 3b demonstrates that, for each $\mathcal{C}$, as the Rayleigh number increases the brine channel spacing L becomes proportional to the depth of the mushy layer h_o.

3. Experimental Validation: Transient Growth

[9] The flux law (2) was derived for convection during steady directional solidification, but growth of sea ice is a transient process forced by the surface flux balance that determines the surface temperature. Therefore, we test our flux law using experimental measurements during transient growth. *Wettlaufer et al.* [1997] solidified sodium chloride solution and natural sea water in a closed system containing a growth cell of depth H with a cooled upper boundary of temperature T_B (and hence liquid salinity $C_B = -T_B/\Gamma$ at local thermodynamic equilibrium). The far field liquid salinity $C_l(t)$ evolved over time as a result of rejection of brine from the growing ice layer of thickness $h(t)$. The flux law (2) can be used in conjunction with an integral salt budget to estimate $C_l(t)$ theoretically for comparison to the laboratory data.

[10] The initial salinity is $C_l(0) = C_0$ and it was observed that the liquid region remained well mixed with uniform salinity. Hence, solute conservation in the liquid region yields a flux

$$\frac{d}{dt}[(C_l - C_0)(H - h)] = F. \tag{3}$$

For transient growth from a fixed-temperature boundary the relevant global mushy layer Rayleigh number is proportional to the mushy layer depth h so that we can identify

$$R_m \sim R_T = \frac{\rho_0 g \beta (C_B - C_l) \Pi_0 h}{\mu \kappa} \tag{4}$$

in (2) and hence

$$F \sim \gamma \frac{\rho_0 g \beta (C_B - C_l)^2 \Pi_0}{\mu} \left(1 - \frac{h_c}{h} \right), \quad \text{for } h > h_c, \tag{5}$$

where $h = h_c$ is defined by $R_T = R_c$.

[11] When the layer thickness is far beyond critical but much smaller than the experimental cell depth ($h_c \ll h \ll H$) then (3) and (5) can be approximated by

$$H \frac{d}{dt}(C_l - C_0) = \gamma \frac{\rho_0 g \beta (C_B - C_l)^2 \Pi_0}{\mu}. \tag{6}$$

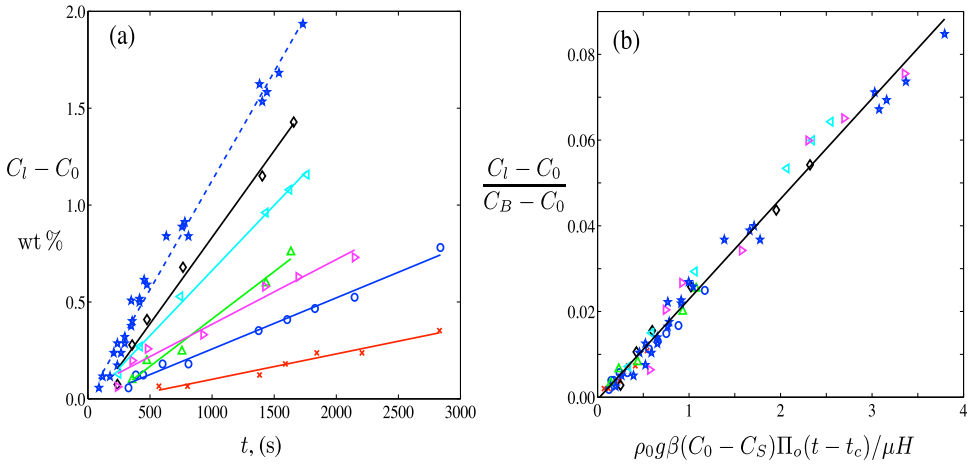

Figure 4. (a) Change in liquid salinity $C_l - C_0$ as a function of time t, for a range of initial liquid salinities and upper boundary temperatures: $C_0 = 1$ wt%, $T_B = -20$°C (red ×), $C_0 = 2$ wt%, $T_B = -20$°C (blue ○), $C_0 = 3.5$ wt%, $T_B = -20$°C (green △), $C_0 = 7$ wt%, $T_B = -20$°C black ◇), $C_0 = 7$ wt%, $T_B = -15$°C (cyan ◁), $C_0 = 7$ wt%, $T_B = -10$°C (magenta ▷), $C_0 = 10.5$ wt%, $T_B = -20$°C (blue ⋆) Data from *Wettlaufer et al.* [1997]. Each data set is consistent with a linear variation of C_l over time, as shown by the lines of best fit. (b) Same data as in Figure 4a, but plotted as dimensionless liquid salinity $(C_l - C_0)/(C_B - C_0)$ versus dimensionless time $\rho_0 g\beta\ (C_0 - C_S)\Pi_0(t - t_c)/\mu H$. The critical time for onset of brine drainage, t_c is known for each data set so that brine drainage commences at dimensionless time zero. We use a value $\Pi_0 = 2 \times 10^{-8}$ m^2 for the reference permeability, using the permeability function of *Notz and Worster* [2009] and $H = 0.376$ m. The data is collapsed by equation (8), with $\alpha = 0.023$.

Moreover, when $C_l - C_0 \ll C_B - C_0$ the solution is approximated as

$$C_l - C_0 \sim \gamma \frac{\rho_0 g \beta \Pi_0}{\mu H}(C_B - C_0)^2(t - t_c), \tag{7}$$

which predicts that the salinity increases linearly in time. Figure 4a plots measured values of $C_l(t)$ for a range of initial salinities C_0 and boundary temperatures T_B. Each data set is described by linear best fit lines, with differing slopes due to the dependence of the prefactor γ on $\mathcal{C}$. Making the hypothesis that $\gamma \sim \alpha\mathcal{C}$ for $\mathcal{C} \ll 1$ with α constant, (7) yields

$$\frac{C_l - C_0}{C_B - C_0} \sim \alpha \frac{\rho_0 g \beta \Pi_0}{\mu H}(C_0 - C_S)(t - t_c). \tag{8}$$

Figure 4b shows that all of the previous data collapses to a single line given by equation (8) with $\alpha = 0.023$. Moreover, a power law fit of $C_l - C_0 \propto (t - t_c)^n$ yields $n = 1.07 \pm 0.05$. This provides confidence that equations (2) or (5) can be applied to describe both transient growth of sea ice (with $\mathcal{C} \ll 1$), and steady state growth. Note that equation (5) predicts that the brine flux does not depend directly on the growth rate V for solidification from a fixed temperature surface. Finally, we note that although the factor α could in principle depend on the parameters θ_∞, $\mathcal{S}$ and Da, the experimental collapse in Figure 4b shows such dependencies are insignificant for freezing conditions in the experiment.

4. Conclusions

[12] The combination of theoretical modeling and test against experiment provide a physically based framework for understanding brine fluxes from growing sea ice. In this manner the brine flux laws emerge from a variational principle underlying the coupling between phase change and fluid flow in the theory of mushy layers. This principle sets the spacing of brine channels to maximize the flux emerging from a growing layer. The resulting scaling law equation (2) successfully reproduces the evolution of liquid salinity in transient growth experiments with a prefactor $\gamma = \alpha\mathcal{C}$, providing further support for the hypothesized variational principle. Importantly, the agreement with both steady state and transient growth implies that equation (2) or (5) *and* experiments provide a general test bed for parameterization of brine fluxes. Moreover, because all values are physically determined our approach removes the need to tune unknown parameters and hence the scaling (2) can easily be applied to estimate brine fluxes in more complex simulations of ice–ocean interaction. Indeed, this motivates present work to determine whether the asymptotic limit $\gamma \sim \alpha\mathcal{C}$ with $\mathcal{C} \ll 1$ can also be recovered via theoretical models of mushy layer growth.

[13] We have calculated the temperature, solid fraction and velocity profiles using the basic underlying conservation laws of the system (Figure 2) and in so doing (a) predict regions of low solid fraction consistent with several basic structural features of observed sea ice, including the "skeletal layer" adjacent to the ice-water interface and the high permeability region close to the brine channel walls where feeder channels for primary brine channels are seen [*Lake and Lewis*, 1970] and (b) detail the nature of the convective exchange of fluid between the ocean and sea ice and hence the resulting influence on its structural properties. Our approach shows that brine drainage occurs via convective cells of order-one aspect ratio for a wide range of $\mathcal{C}$ values, consistent with the region of gravity drainage, substantially larger than the skeletal layer, observed adjacent to the ice water interface by *Notz and Worster* [2009]. The resulting exchange is likely to control the overall transfer of gases and other tracers of relevance to biogeochemical processes through the sea ice cover. Therefore, the combination of the brine flux scaling equation (2) and structural details described

via mushy layer theory provide the basic theory for a thermodynamic model of sea ice that predicts rather than prescribes brine transport dynamics.

[14] **Acknowledgments.** We thank the U.S. National Science Foundation grant OPP0440841 and Yale University under the Bateman endowment for support of this research, and along with Eric Rignot thank two anonymous reviewers.

References

Adams, J. C. (1989), Mudpack: Multigrid portable fortran software for the efficient solution of linear elliptic partial differential equations, *Appl. Math. Comput.*, *34*, 113–146.

Briggs, W. L., V. E. Henson, and S. F. McCormick (2000), *A Multigrid Tutorial*, SIAM, Philadelphia, Pa.

Chung, C., and M. G. Worster (2002), Steady-state chimneys in a mushy layer, *J. Fluid Mech.*, *455*, 387–411.

Comiso, J. C. (2003), Large-scale characteristics and variability of the global sea ice cover, in *Sea Ice: An Introduction to its Physics, Chemistry, Biology and Geology*, edited by D. N. Thomas and G. S. Dieckmann, pp. 112–142, Blackwell, Malden, Mass.

Cox, G., and W. F. Weeks (1988), Numerical simulations of the profile properties of undeformed first-year sea ice during the growth season, *J. Geophys. Res.*, *93*, 12,449–12,460.

Eide, L., and S. Martin (1975), The formation of brine drainage features in young sea ice, *J. Glaciol.*, *14*, 137–154.

Feltham, D. L., N. Untersteiner, J. S. Wettlaufer, and M. G. Worster (2006), Sea ice is a mushy layer, *Geophys. Res. Lett.*, *33*, L14501, doi:10.1029/2006GL026290.

Foster, T. D. (1969), Experiments on haline convection induced by freezing of sea water, *J. Geophys. Res.*, *74*, 6967–6974.

Katz, R. F., and M. G. Worster (2008), Simulation of directional solidification, thermochemical convection, and chimney formation in a Hele-Shaw cell, *J. Comput. Phys.*, *227*, 9823–9840.

Lake, R., and E. Lewis (1970), Salt rejection by sea ice during growth, *J. Geophys. Res.*, *75*, 583–597.

Neufeld, J. A., and J. S. Wettlaufer (2008), Shear-enhanced convection in a mushy layer, *J. Fluid Mech.*, *612*, 339–361.

Notz, D., and M. G. Worster (2009), Desalination processes of sea ice revisited, *J. Geophys. Res.*, *114*, C05006, doi:10.1029/2008JC004885.

Notz, D., J. S. Wettlaufer, and M. G. Worster (2005), A non-destructive method for measuring the salinity and solid fraction of growing sea ice in-situ, *J. Glaciol.*, *51*, 159–166.

Schulze, T. P., and M. G. Worster (1998), A numerical investigation of steady convection in mushy layers during the directional solidification of binary alloys, *J. Fluid Mech.*, *356*, 199–220.

Schulze, T. P., and M. G. Worster (2005), A time-dependent formulation of the mushy-zone free-boundary problem, *J. Fluid Mech.*, *541*, 193–202.

Solomon, T., and R. Hartley (1998) Measurements of the temperature field of mushy and liquid regions during solidification of aqueous ammonium chloride, *J. Fluid Mech.*, *358*, 87–106.

Tait, S., and C. Jaupart (1992), Compositional convection in a reactive crystalline mush and melt differentiation, *J. Geophys. Res.*, *97*, 6735–6756.

Thomas, D. N., and G. S. Dieckmann (Eds.) (2010), *Sea Ice*, 2nd ed., Blackwell, Oxford, U. K.

Untersteiner, N. (1968), Natural desalination and equilibrium salinity profile of perennial sea ice, *J. Geophys. Res.*, *73*, 1251–57.

Vancoppenolle, M., T. Fichefet, H. Goosse, S. Bouillon, G. Madec, and M. Maqueda (2009), Simulating the mass balance and salinity of Arctic and Antarctic sea ice. 1. Model description and validation, *Ocean Modell.*, *27*, 33–53.

Wakatsuchi, M., and N. Ono (1983), Measurements of salinity and volume of brine excluded from growing sea ice, *J. Geophys. Res.*, *88*, 2943–2951.

Wakatsuchi, M., and T. Saito (1985), On brine drainage channels of young sea ice, *Ann. Glaciol.*, *6*, 200–202.

Weeks, W. F. (2010), *On Sea Ice*, Univ. of Alaska Press, Fairbanks.

Wells, A. J., J. S. Wettlaufer, and S. A. Orszag (2010), Maximal potential energy transport: A variational principle for solidification problems, *Phys. Rev. Lett.*, *105*, 254502, doi:10.1103/PhysRevLett.105.254502.

Wettlaufer, J. S., M. G. Worster, and H. E. Huppert (1997), Natural convection during solidification of an alloy from above with application to the evolution of sea ice, *J. Fluid Mech.*, *344*, 291–316.

Worster, M. G. (1992), Instabilities of the liquid and mushy regions during solidification of alloys, *J. Fluid Mech.*, *237*, 649–669.

S. A. Orszag, Department of Mathematics, Yale University, New Haven, CT 06520-8283, USA.

A. J. Wells and J. S. Wettlaufer, Department of Geology and Geophysics, Yale University, New Haven, CT 06520-8109, USA. (andrew.j.wells@yale.edu)